Quasi Biennial Oscillation Impacts on Madden Julian Oscillation-Associated Tropical

Extratropical Interactions and Kelvin Waves

Paul E. Roundy, Department of Atmospheric and Environmental Sciences, University at Albany,

State University of New York, Albany, New York

Corresponding Author Email: proundy@albany.edu

1

Abstract

Several recent works have demonstrated that the Madden Julian oscillation (MJO) shows more variance in tropical convection and wind during the easterly phase of stratospheric wind in the quasi biennial oscillation (QBO). Some of these works have shown that reduced variance during the westerly QBO is associated with fewer repeating cycles of events. This paper applies a modulation linear regression algorithm to assess changes in the global atmospheric circulation structure for December through February MJO signals tested when time-smoothed 50 hPa winds are easterly or westerly at 10 m s⁻¹. Results show pronounced differences in the associated extratropical upper tropospheric Rossby wave response between the two QBO states, along with a comparatively lower fraction of total eastward wave energy being consistent with Kelvin waves approaching the Indian basin from the west during the westerly QBO. Instead, westerly QBO appears to favor stronger equatorward-moving extratropical wave precursors across the Western Hemisphere and Eurasia. The results suggest the hypothesis that more dependence on extratropical waves during the westerly QBO may reduce the reliability of the MJO to form sequential trains during the westerly QBO.

Key Words:

Madden Julian oscillation, quasi biennial oscillation.

1. Introduction

Subseasonal anomalies of deep convection frequently organize and evolve eastward across the tropical warm pool regions, together with a circulation signal that transits the globe. Such signals have become known as the Madden Julian oscillation (MJO, Madden and Julian 1972, Zhang 2005), the leading subseasonal mode of the tropical atmosphere. Recently, several authors have described how variance in the MJO tends to be largest during the easterly phases of the quasi biennial oscillation (QBO) (Yoo and Son 2016, Zhang and Bosong 2018, Martin et al. 2019, Densmore et al. 2019; Sakaeda et al. 2020). For a review, see Martin et al. (2021). The QBO is a roughly 26-month fluctuation of alternating descending regions of anomalous zonal mean zonal wind in the equatorial stratosphere. The QBO is generated as damped Kelvin and gravity waves deposit momentum near the shear layer that divides the two regions (e.g., Plumb and Bell, 1982). Yoo and Son (2016) and others argue that the relationship between the MJO and the QBO may be associated changes in the stratification of the upper troposphere driven by the QBO. Klotzbach et al. (2019) demonstrate that this difference in the variance between the easterly and the westerly phases of the QBO has been apparent only since about 1980. They argue that changes in the upper tropospheric static stability, associated with raising of the tropopause associated with the changing climate, have yielded this development of the MJO-QBO relationship. Hood et al. (2020), Toms et al. (2020), and Feng and Lin (2019) show significant differences between extratropical atmospheric circulation patterns associated with the MJO in opposite QBO states, highlighting especially differences in patterns associated with the North Atlantic Oscillation (NAO). Some of these differences are attributed to the changes in the amplitude of the forcing due to weaker convection during the westerly phase of the QBO, or to better organization of the wave train response to MJO convection due to a better organized west Pacific subtropical jet stream during

the westerly QBO. Feng and Lin (2019) also suggest that enhanced mid latitude westerlies during the westerly QBO might enhance upward propagation of Rossby waves that then influence the NAO. Mayer and Barnes (2020) showed that prediction skill in the mid latitude atmospheric circulation is significantly enhanced associated with MJO events in strong QBO states, with especially enhanced skill during the westerly QBO.

The MJO circulation constitutes a vast network of equatorial and extratropical Rossby waves (e.g., Roundy and Frank 2004; Roundy 2014; Sakaeda and Roundy 2015), Kelvin waves (Weare 2010; Roundy 2019; Haertel 2021), overturning circulations, and breaking waves (e.g., Moore et al. 2010; MacRitchie and Roundy 2016). There is evidence that these signals collectively circumnavigate the world, either directly through traceable individual disturbances, or through enhancements and reductions of their overall variance that evolve eastward. The range of wavelike features and breaking wave features that evolve with the MJO collectively interfere with each other, ranging from fast, dry, stratospheric Kelvin waves moving eastward more rapidly than 30 ms⁻¹, to convectively coupled Kelvin waves often moving eastward at 10-20 ms⁻¹ (Straub and Kiladis 2003; Roundy 2008), to Kelvin and Rossby wave features over the warm pool directly associated with the MJO convection itself, acting on its own favored scales and phase speeds (e.g., Roundy 2019), to quasi stationary zonally narrower features associated with breaking waves as the MJO intersects with exit regions of the subtropical jet stream (e.g., MacRitchie and Roundy 2016), to westward-moving equatorial Rossby waves forced by coupling of the MJO with the extratropics, monsoons, or even the Rossby gyres left behind after MJO convection weakens (e.g., Roundy and Frank 2004; Wang and Xie 1997). The equatorward sides of Rossby gyres exhibit the opposite pressure wind relationships to Kelvin waves, so their presence is indicated by easterlies aligned with ridge anomalies, or the opposite. A portion of intruding extratropical Rossby waves or breaking waves become quasi stationary (depending on the balance between their intrinsic phase speeds and the background wind), producing more persistent non propagating anomalies associated with the MJO. The mix of free Rossby and Kelvin waves must become dominated by Kelvin waves as the disturbances move from west to east from the region of upper tropospheric westerlies to upper tropospheric easterlies, where Rossby waves cannot freely propagate eastward. It is not surprising, therefore, that although it is clear that signals associated with the MJO circumnavigate the globe, its coexistence with features including stationary and propagating signals across a wide spectrum from westward to standing to rapid eastward propagating implies that individual and composite MJO events will show interference patterns instead of smoothly eastward circumnavigating features. The spectrum of such features that interact with the MJO circulation signal may vary with the QBO, including both tropical and extratropical features that apparently translate MJO-associated circulation signals around the world.

This paper analyzes the differences in upper tropospheric circulation signals in the December through February MJO between symmetrically defined states of the easterly and westerly phases of the QBO. As with the above papers, there are plausible mechanisms that might lead to anticipate differences in the characteristics of the MJO-associated atmospheric circulation patterns between these two regimes. The QBO zonal wind fluctuation is largely confined to the equatorial region. Although the wave-mean flow interaction mechanisms that propagate the QBO downward in the stratosphere may at times be present in the troposphere, other mechanisms active in the troposphere create a consistent contrast between the equatorial stratospheric zonal wind and the tropical troposphere. For example, vertical mixing by moist deep convection in the troposphere reduces the amplitude of signals generated by gradual deposition of momentum by breaking waves there (e.g., compare the scales of convective momentum transports, such as by Richter and Rasch

2008 with accelerations achieved by acceleration rates associated with the QBO, of order 10⁻⁷m s⁻²). The extratropical stratosphere and troposphere also cannot sustain QBO-like fluctuations (Haynes 1998), so evolution of the QBO across its phases must create shear contrast between the QBO zonal wind fluctuation and the regions poleward and below, leading to changes in vertical and meridional shear between the equatorial stratosphere and surrounding regions. These patterns of changing wind shear can be expected to alter the propagation of Kelvin waves along the equator and Rossby waves into and out of the tropics. Since MJO convection is an active Rossby wave source, radiating waves across the world from its regions of upper tropospheric mass divergence driven by deep convection and interacting with vorticity gradients, it is reasonable to anticipate that Rossby waves associated with the MJO may refract differently into the extratropics during opposite QBO states. Since Rossby waves moving toward the equator also impact MJO-associated circulations in the Western Hemisphere and proximate to Africa (e.g., Roundy 2014; Sakaeda and Roundy 2015; Gahtan and Roundy 2020a,b), the QBO may also impact the evolution of the Rossby wave component of the MJO's response pattern that propagates back into the tropics. This extratropical Rossby wave radiation back into the tropics may be relevant for the translation of the MJO signal around the world to initiate secondary events (e.g., Roundy 2014; Sakaeda and Roundy 2015). The composite MJO signal is also associated with a pronounced upper tropospheric Kelvin wave (Roundy 2020), which, although probably not strictly necessary for evolution of the MJO circulation signal around the world, likely would facilitate its translation around the world and subsequent development of new MJO convection over the Indian Ocean (e.g., Powell and Houze 2015). Along the equator, the MJO-associated Kelvin wave dominates the eastward-moving signal associated with the MJO in regions of upper tropospheric easterly wind, while Kelvin waves mix with eastward-moving Rossby waves in regions of westerly wind, implying mixed signals driven

by different mechanisms in the Western Hemisphere (Roundy 2014, Sakaeda and Roundy 2015). The change in vertical shear of the zonal wind associated with the QBO may thus impact the extent to which MJO-associated Kelvin wave energy is retained in the upper troposphere as the MJO translates the Western Hemisphere, while the change in horizontal wind shear across the subtropics may affect the radiation of Rossby waves into and out of the tropics.

This paper applies a modulation linear regression algorithm adapted from Roundy (2017) to assess the expectation value of MJO-associated upper tropospheric circulation patterns during opposite QBO states. The regression approach allows us to approximately diagnose the favored MJO atmospheric circulation signal in specific selected QBO states, as opposed to the usual approach of applying composites or regression analysis during periods of time characterized by a range of background states.

2. Data and Methods

2.1 *Data*

2.5-degree daily mean OLR data (Liebmann and Smith, 1996) from the National Oceanic and Atmospheric Administration (NOAA) serve as a rough proxy for convection. 200 hPa Geopotential height and wind data are obtained from the ERA5 reanalysis, and 50 hPa wind data, smoothed with a 3-month centered moving average, are used to track the QBO. These datasets are found at

https://www.esrl.noaa.gov/psd/data/gridded/data.interp OLR.html and

https://www.ecmwf.int/en/forecasts/datasets/reanalysis-datasets/era5

The seasonal cycle including the first three harmonics are subtracted from each variable, using the climatology of 1979-2020. To fill the full period, the interpolated OLR data were padded on the end with NOAA uninterpolated OLR data, which were then interpolated by replacing missing data

with the average value of available anomalies from all directly neighboring grid points along with the same and neighboring grid points from the day before to the day after.

2.2 Regression Analysis

Linear regression analysis is frequently applied to diagnose patterns associated with base indexes chosen to represent phenomena like the MJO. A field of grid points of predictand time series Y (in this case, from which the time mean and seasonal cycle have been subtracted) is related to the similarly centered predictor index X through the relation Y = XC, where C, in this centered linear case, is a vector of regression slope coefficients corresponding to each grid point in Y. At each grid point, C is the ratio of the covariance between the time series from Y and the time series X divided by the variance of X. When calculated during different periods of time in different background conditions, the coefficients vary. Roundy (2017) developed a method of linear regression that allows computation of C as it varies continuously with a background variable. In the case of Roundy (2017), the background variable was the seasonal cycle. The algorithm uses a regression inside a regression, effectively predicting the relevant variance and covariance quantities as they vary with the harmonics of the seasonal cycle. In this paper, the algorithm is modified to replace the seasonal cycle harmonics with a new matrix consisting of a column of ones and an index of 50 hPa zonal mean zonal wind averaged from 5°N to 5°S and smoothed with a 3month centered moving average (as an index of the QBO).

Simple linear regression approaches with only the slope term diagnose only the linear component of the target variability. When applied to data from phenomena with nonlinear statistics (for example, positive or negative phases with somewhat different shapes), the linear approach will diagnose the part of the signal that reflects linearity. This linearization of the flow, or projection of the whole signal onto a linear model, represents a real signal, but can omit other

important parts of the flow. Adding nonlinear terms to a regression model (e.g., Roundy and Frank 2004) can diagnose nonlinear components of the signal, but such terms can also cause overfitting, especially in the modulation regression context considered here. As with all applications of linear regression to atmospheric phenomena, the caveat that some of the flow may be omitted must be considered.

Following several works cited in Section 1, which have demonstrated that the MJO asymmetry with the QBO occurs predominantly during northern winter, only data centered on December through February are included in the analysis. Since the present work focuses on mechanisms not included in those previous works, there is good motivation to extend this type of analysis to other seasons as well, but was avoided here for brevity. Results are made by separately constructing regression maps based on the real time multivariate MJO (RMM) index of Wheeler and Hendon (2004). Although the index does not represent all signals in the MJO, nor does it represent only MJO (e.g., Roundy et al., 2009), it has demonstrated usefulness in assessing bulk MJO structure and propagation characteristics. Results for RMM1 and RMM2 are then linearly combined to reconstruct the signals associated with the eight canonical MJO phases. A caveat of application of the RMM index in this case is that it depends on fixed spatial structures that may not be exactly the same if assessed separately for easterly and westerly phases of the QBO.

Statistical significance of the regression analysis is assessed via a Monte Carlo experiment based on creating random indexes with the same power spectrum as the RMM index, and repeating the full analysis based on random indexes 1000 times. The repeated regressions generate null distributions of each variable at each grid point. The regressed result at a given grid point is deemed statistically different from zero when it sits outside of the centered 95% confidence interval of regressed values generated from the random data. The results for QBO easterly and QBO westerly

phases are deemed statistically different from each other when the difference between them is larger than the appropriate confidence interval of the null distribution constructed from the random indexes. The approach is similar to that applied by Roundy (2019) and by Elsner and Tsonis (1993). The same null distribution is also applied to diagnose the 95% confidence levels for difference from zero in each variable.

Since the regression algorithm is relatively new, a composite analysis is applied here to verify the regression results. The approach averages data over a set of dates when certain conditions are met, to diagnose the expected patterns under those conditions. This demonstration uses the union of all RMM phase 7 days of amplitude greater than 0.5 during December through February when the 50 hPa QBO index is either less than -4 m s⁻¹ or greater than +4 m s⁻¹. These qualifiers were selected in order to generate a list of dates sufficiently long that the results are statistically stable, but sufficiently short that the results map toward the same part of the vector space targeted by the regression analysis. Phase 7 is used because it shows some of the most pronounced global differences in MJO-associated signals between easterly and westerly QBO, as suggested by the regression analysis. Statistical significance of the difference from zero of the composite anomalies is assessed through a student's t-test, at the 95% confidence level. A similar test for difference between the two QBO states was also performed as to that in the regression analysis, with similar results, and significance of the difference from zero was also applied to the regressions, but not shown. Showing significance in this way between the regressions and composites was intended to provide a representative result from both types of tests while not over cluttering the maps.

3. Results

3.1 Overview of Regression Results

Regressed 200 hPa winds and geopotential height anomalies for RMM phases 5-8 are shown in Figures 1 through 4 during the 10 m s⁻¹ easterly QBO (Panels a) and the 10 m s⁻¹ westerly QBO (Panels b). Given the symmetry implicit in linear regression on centered data, phases 1-4 are equal but opposite in sign to the results for phases 5-8, so phases 1-4 are not shown. Figure 5 shows the same results in the longitude-phase domain, averaged from 10°N to 10°S. The base indexes are set at 2 standard deviations for index data from December through February, projecting a major event, but one of consistent index amplitude between the two QBO states. This approach allows for comparison of equal RMM amplitude events between the two equal amplitude QBO states. Thus, amplitude and structural differences diagnosed reflect only the association with the QBO. Although the QBO itself is not symmetric between its easterly and westerly states, this imposition of symmetry suggests from the data what equal and opposite QBO states would yield, given equal RMM index amplitude between them (which facilitates comparison between structures associated with the events).

3.2 Similar Regressed Features between QBO Easterly and Westerly States

In both QBO states, bulk similarities appear in the results for each phase. The main bodies of negative and positive OLR anomalies shown in the shading in Figures 1-4 occur at roughly the same locations. Easterly wind anomalies appear on the equator within and to the west of the convection (accounting for sign reversal given opposite phases) with westerly anomalies within and to the west of the regions of anomalously suppressed convection. Where OLR anomalies are strongest, such as the positive anomalies over the Indian Ocean during phase 7 or the negative anomalies over the West Pacific during phase 6, trough anomalies appear in the subtropics near

and west of the positive anomalies with ridge anomalies near and west of the negative anomalies. Trains of alternating positive and negative height anomalies extend around the world from the negative and positive OLR anomalies. As the equatorial wind anomalies progress around the world in the tropics, they tend to broaden zonally through the Western Hemisphere and narrow through the eastern (e.g., during phase 7, Fig. 3, equatorial westerlies extend from near 140°W to 90°E, while the corresponding region of easterly wind is isolated between 140°E and 180). This signal in the zonal wind data is also shown in Figure 5 at phases 5-7, which broadly suggests equatorial westerly wind over most of the region from roughly 150°W to 100°E, with a narrower signal of much slower eastward propagation of easterly wind anomaly from roughly 100°E to 160°E. This type of slowing and narrowing of the signal would occur in response to advection by upper tropospheric easterly background wind over the warm pool and by westerly background wind through the Western Hemisphere, in addition to any effect of convection slowing the signal down over the Indian Ocean (See Sakaeda and Roundy 2015, especially their Figure 1).

Although the zonal wind anomalies appear to more smoothly circumnavigate the world (Figure 5), the long zonal scale in the Western Hemisphere height anomalies is broken by Rossby waves intruding on the westerlies (see also Moore et al. 2010, Sakaeda and Roundy 2015, Roundy 2014, MacRitchie and Roundy 2016). These intrusions appear as zonally narrow reversals of height anomalies relative to those to their east and west that flip sign as RMM phase progresses (e.g., Fig. 5 near 80°W). These intrusions make it impossible to see any continuous pure Kelvin wave propagation across the Western Hemisphere. An example intrusion event occurs over the Central Pacific Ocean during RMM phases 3-4 (see the opposite signal in Figs. 3-4, or phases 3-4 shown in Fig. 5). There, a westerly wind anomaly develops in a geopotential trough anomaly (e.g., Fig. 5a). The relevant map is Figure 3, which, multiplied by -1, yields the corresponding map for

RMM phase 3. Similar to MacRitchie and Roundy (2016), the resulting map has a trough anomaly introduced into the region southwest of Hawaii. They showed that this structure occurs in MJO events that include Rossby wave breaking near Hawaii, but not in events that do not include wave breaking there. Most events include such wave breaking. The resulting upper tropospheric trough anomalies accelerate westerlies on their equatorward sides, in a pressure wind pattern opposite that expected for Kelvin waves. The associated gyre pattern does not tend to propagate eastward, but remains quasi stationary as a blocking pattern through phase 4 as the MJO signal continues to advance. Similar breaking wave signals occur with the MJO from that region eastward to Africa. The more consistent phasing between height and wind anomalies over the Indian Ocean, their cross-equatorial symmetry, and their projection onto wavenumber 1-2 are all consistent with Kelvin wave signal over the Indian Ocean, a substantial portion of which may arrive from the west. However, a portion of that Kelvin-like signal may also form in situ, possibly triggered by extratropical Rossby waves following the mechanism suggested by Sakaeda and Roundy (2015).

However, as this bulk envelope of mixed Kelvin and Rossby wave signal progresses eastward over Africa toward the Indian basin, background wind swaps from westerly to easterly, so that this region must serve as a filter, allowing only free Kelvin waves to occur and preventing stationary Rossby waves associated with breaking extratropical waves. Thus, over Africa and the Indian Ocean, geopotential height anomalies (shown in shading) are largely in phase with zonal wind anomalies. Proximate to and just east of the Dateline, the correlation between equatorial height and wind anomalies locally reverses where Rossby waves break into the tropics near the West Pacific jet exit region (Figures 1, 3, and 4, but see also Figure 5).

3.3 Differences between Easterly and Westerly QBO

Pronounced differences occur around the world between the two QBO states, dominated by phase shifts and amplitude differences of the regressed wind and geopotential height anomalies. For regions of significantly different geopotential height anomalies, Table 1 shows the global mean squared regressed anomalies for each RMM phase. Westerly QBO is associated with values 2-6 times higher than for easterly QBO, with the greatest difference during phases 1 and 5 and the smallest during phases 2 and 6. Since squared height anomalies are larger in the mid to high latitudes, this difference is dominated by those regions. The regions of statistically significant differences between the results for QBO easterly and westerly states vary by phase. During phase 5 (Fig. 1b) during westerly QBO, significantly stronger ridge anomalies occur along a rough line from near the equator and 90°W to 35°N and 30°W, to 35°E and 35°N, to between 90°E and the Dateline near 60°N. Also during phase 5, a significant trough anomaly occurs over the North Atlantic region near 60°N. During phase 6 (Figure 2b), the ridge anomaly previously near 35°E during phase 5 erupts poleward to eastern Scandinavia and Western Russia. During phases 7 and 8 (Figs. 3-4, panels b), this ridge centers westward, developing a significantly stronger block in the North Atlantic basin, with the block pattern including a significantly stronger trough anomaly south of the North Atlantic ridge that extends from 45°N southward across the tropics. During phases 5-6 (Figs. 1-2), more of the regions of significant differences occur at high latitude, while during phases 7-8 (Figs. 3-4), greater geographic extent of significantly different height anomalies occurs in the tropics, especially from the Atlantic basin eastward across Africa.

Along the equator, these statistically significantly stronger trough anomalies over the South America and the Atlantic region during phase 7 and over South America east to across Africa during phase 8 extend to the equator except in a few regions of Kelvin-wave like ridge anomalies embedded in the broader westerly anomalies (Fig. 3b). Elsewhere along the equator, *relative* trough anomalies collocated with easterly wind anomalies and ridge anomalies with westerly wind anomalies occur during the easterly phase of the QBO, but are statistically significantly different from zero over substantially smaller regions during the westerly QBO (e.g., phase 5-6, or Figs. 1-2, over the Indian Ocean, phase 6 over S. America, the eastern Atlantic basin, Africa, and the Western Indian Ocean, and during phase 8 over Africa and the Indian Ocean, difference from zero not shown). Equatorial ridge anomalies collocated with westerlies are not statistically different from each other between easterly and westerly QBO, but the greater incursion of trough gyres toward the equator over the Atlantic and Africa superimposed on the regions of Kelvin-like ridges appears to shrink the extent of the significant Kelvin ridge signals in equatorial westerlies (e.g., Figures 2-3 near the equator over South America and Africa). This result suggests that differences in signals consistent with Rossby waves, especially those associated with the enhanced North Atlantic block during westerly QBO, dominate changes in the balance between Kelvin waves and Rossby waves during the Westerly QBO.

3.4 Equatorial Longitude-phase Domain

Figure 5 shows the longitude-time domain results for easterly QBO (a), westerly QBO (b), and easterly QBO minus westerly QBO (c). Since phases can last different amounts of time between the two QBO states, no specific inference can be made with respect to comparison of phase speed from these diagrams, but the results are useful to illustrate the zonal-temporal chronologies of phasing between regressed zonal wind and geopotential height anomalies. Shading in panels a and b shows globally similar zonal wind anomalies, with upper tropospheric easterly wind anomalies emerging over Africa and the Indian Ocean during phase 2, with westerlies slowly moving eastward over the Maritime Continent and West Pacific region at the same time. These

westerly wind anomalies then move rapidly eastward, interrupted by narrower regions of easterly wind anomalies across the Western Hemisphere. Roundy (2014) and Sakaeda and Roundy (2015) have argued that this Western Hemisphere signal constitutes a mix of Rossby wave and Kelvin wave energy propagating eastward together in background westerly wind. During the easterly QBO, although height anomalies in the Western Hemisphere alternate phase with zonal wind anomalies, the average Western Hemisphere pattern has easterlies collocated with trough anomalies and westerlies collocated with ridges. During the westerly QBO, except for the region just west of the dateline, the strongest zonal wind anomalies of either sign are collocated with somewhat weaker height signals of the same sign, with a few regions that include signals of opposite sign between height and wind anomalies. The pattern of more opposite-signed height anomalies with wind anomalies suggests that the fraction of Kelvin versus Rossby wave action there favors the Rossby wave. Figure 5 thus suggests that communication of the MJO signal eastward across the Western Hemisphere to the Indian Ocean has a more substantial fraction of its variance in the Kelvin wave component during the easterly QBO, but that the extratropical Rossby wave component, including ridges or troughs breaking onto the equator, is more prominent with eastward translation of the MJO zonal wind anomaly during the westerly QBO. This extratropical translation mechanism does not express itself as continuous translation across the tropics, because of quasi-stationary blocking components that reverse across the MJO circuit but that do not themselves propagate eastward continuously (Roundy 2014).

3.5 Comparable Composite Analysis

Figure 6 shows the composites between DJF RMM 7 during QBO index less than –4 m s⁻¹ (panel a) and similar conditions during QBO index greater than –4 m s⁻¹ (panel b), as an example, for comparison against Figure 3. The contour interval of geopotential height anomalies given in

Fig. 6 is half that of Figures 1-4, because Figs. 1-4 defined an event of 2 standard deviations, while Figure 6 had to include events over a wide range of standard deviations in order to achieve a population of events large enough to yield statistical stability. Although it is not expected that the regressions and the composites will be identical, there are pronounced similarities that support the general conclusions of the regression analysis. Regions of statistically significant height anomalies tend to concur. Significance of the difference from zero is shown in Fig. 6 and difference between QBO easterly and westerly is shown in Figs. 1-4, for different reasons. All fields were tested both for difference from zero and for difference between easterly and westerly QBO. Showing them both on all figures cluttered the maps. Particular highlights include a Scandinavian ridge during westerly QBO and a trough during easterly QBO. The ridge over Greenland during easterly QBO extends farther south of Greenland during Westerly QBO, and the ridge anomalies along the equator near South America and Africa during easterly QBO are more encroached upon by significant trough anomalies to the north and south during Westerly QBO. This result compares well with Feng and Lin (2019), their Figure 2, but regressed height anomalies over Greenland in Figure 6 are not deemed statistically different between the QBO states (significantly different anomalies do occur south and east of Greenland, depending on the phase), even though, as suggested by Feng and Lin (2019), the ridge over Greenland is statistically different from zero during RMM phase 7 in the easterly QBO, but not the westerly. A caveat in the comparison is that the regression analysis constrains the amplitude of the two origin RMM signals to be the same, but the composite analysis does not. However, the mean RMM amplitudes between the easterly and westerly QBO were 1.50 and 1.35, so that the two are similar to within about 10%.

3.6 Results Synopsis and Covariance Analysis

Focusing on the tropics from Africa eastward across the Indian Ocean during the easterly QBO, Figures 1-6 suggest a pressure-wind relationship indicative of dominance of Kelvin wave structure proximate to the equator, with cross equatorially symmetric ridge anomalies in phase with zonal wind anomalies. Alignment between equatorial pressure and wind anomalies is a necessary but not sufficient condition to identify Kelvin waves. Yet these patterns also exhibit symmetry across the equator and taper in amplitude toward the poles, as for Kelvin waves. They also appear consistent with global wavenumber 1 to 2, where the Kelvin wave dispersion line intersects the MJO timescale. Kelvin wave dynamics emerge as a consequence of the spatial structure. That is, convergence of the wind redistributes mass, thereby, for example, raising height anomalies east of the ridge. These results are sufficient to argue that Kelvin wave dynamics are probably present, because they emerge directly as a consequence of the spatial patterns. In contrast, between 150°E and 210°E, zonal wind and height anomalies appear to be in quadrature during the westerly QBO. Near 300°E, a local signal shows an out of phase relationship between zonal wind and height anomalies during the easterly QBO, with only a low amplitude signal corresponding during the westerly QBO.

The regression algorithm is not yet widely used, so in order to provide additional independent validation of the general pressure wind relationship in the MJO with the QBO, this paper provides an independent analysis, focused similarly on December through February. This analysis depends on the QBO 50 hPa zonal wind index used above, and a time series at each longitude grid point along the equator (using data averaged from 10°S to 10°N), generated by taking the product of MJO-filtered 200 hPa zonal wind and geopotential height anomalies. The 10°S to 10°N averaging filters for symmetry across the equator, which is a second requirement for

identification of Kelvin waves. The MJO filter is accomplished in the zonal wavenumber frequency domain, following the method of Wheeler and Kiladis (1999) including wavenumbers 0-9 eastward and periods of 20 to 100 days, which includes the Kelvin wave dispersion line at wavenumbers 1-2 as well as Rossby wave features associated with the MJO, including the residual of Rossby wave breaking, which introduces Rossby gyres into the tropics (e.g., MacRitchie and Roundy 2016). The covariance is calculated between the time series of this product at each grid point and the QBO index. A positive covariance would imply that during the westerly QBO, the height and wind tend to be more in phase. A small covariance can imply that the two signals have small correlation (i.e., mixed Rossby and Kelvin-like signals) or have low overall amplitude. Thus, a reduction of negative covariance during easterly QBO can imply some mix of reduced Kelvin wave-like amplitude and a relative increase in Rossby-wave like signal, or reduced overall activity in waves of both types that maintains a similar fraction of both. The algorithm is therefore most useful as an indicator of which wave form a strong covariance signal indicates. Use of covariance instead of correlation allows for consideration of amplitude factors. The approach was repeated based on retaining only wavenumbers 1-2 in the filtered data to find the part of the signal proximate to the Kelvin wave dispersion line.

Figure 7 shows the results. Negative covariances dominate over Africa and the Indian Ocean, where like-signed height and wind anomalies occur in Figure 5a, and where little zonal wind anomalies consistent with Figure 5a occur in the absence of substantial height anomalies. Positive covariances occur between 150°E and 150°W, where height anomalies and wind anomalies are more in phase in Fig. 5b (westerly QBO). Significant positive covariances also occur near 90°W, where a local opposite phase relationship occurs between zonal wind and height anomalies during the easterly QBO. Results are broadly consistent with the results of the regression

analysis on the local dominance of Rossby or Kelvin-like features proximate to the equator around the world during opposite QBO states. The algorithm assesses only the local mix of such properties, not whether the assessed signals arrive at each longitude from the west or develop in situ (see Figure 5 for more insight on this question). Repeating the analysis based on wavenumbers 1-2 alone has a similar large-scale structure (thin curve), with a minimum over the western Indian Ocean and a maximum near the Dateline. Results remain consistent, with variance including only wavenumbers 1-2 being more dominated by Kelvin-wave consistent signals over Africa and the Indian Ocean during the easterly QBO.

4. Conclusions

A modulation-regression algorithm is applied to assess the different patterns of upper tropospheric circulation associated with the MJO during opposite signed 10 m s⁻¹ 50 hPa zonal wind states tracking the easterly and westerly phases of the QBO. Results focus in two general areas; (a) the MJO signals in the midlatitudes or higher, for example signals across the North Atlantic eastward across Eurasia and (b) the balance of Kelvin and Rossby wave components of the MJO within the tropics, especially across the Americas east to the Western Indian Ocean. Results addressing (a) generally support previous results. Feng and Lin (2019), Hood et al. (2020), and Toms et al. (2020) had previously demonstrated an association between the QBO and the NAO signal associated with the MJO. The present results and Figure 2 of Feng and Lin (2019) suggest a meridional shift in the phasing of the NAO-associated height anomalies. Greenland ridge anomalies associated with the MJO during the easterly phase of the QBO are statistically different from zero (Fig. 6a), but not during the Westerly phase (Fig. 6b), when the significant ridge instead tends to occur just south of Greenland. Although the present results are consistent with Feng and Lin (2019), the ridge anomaly over Greenland failed to show significant difference between the

opposite QBO states. Feng and Lin (2019) only assessed difference from zero. In any case, the present results suggest substantially stronger 200 hPa height anomalies across the North Atlantic basin and Eurasia, in an alternating wave pattern that enters the tropics of Africa Asia, and the Indian basin.

With respect to (b), previous works have shown that the globally evolving circulation signal associated with the MJO contains tropical (mostly Kelvin wave) and extratropical Rossby wave components (e.g., Roundy 2014). The results of this work suggest that the Rossby wave component is relatively stronger than the Kelvin component during the westerly QBO, and the Kelvin wave component is more significant during the easterly QBO. The equatorial zonal wind anomalies associated with the MJO are not broadly significantly different between easterly and westerly QBO (not shown), but the height differences are. Western Hemisphere tropical upper tropospheric circulation patterns associated with the MJO include both Kelvin and eastwardadvected Rossby wave components, making it difficult to track a pure Kelvin signal across the Western Hemisphere (Roundy 2014, Sakaeda and Roundy 2015). As these signals progress eastward toward Africa, reversal of upper tropospheric background wind from westerly to easterly allows for the Kelvin component to continue eastward while filtering out the Rossby wave signal. This difference results in substantial westerly wind over Africa in phase with upper tropospheric ridge, consistent with Kelvin waves, arriving over the Indian Ocean at the time of onset of the MJO suppressed convection there, during the easterly QBO, but these westerlies arrive over Africa with significant ridge anomalies during the westerly QBO extending over substantially smaller geographical area as geopotential trough gyres apparently linked to the North Atlantic blocking encroach closer to the equator. The opposite occurs leading to the Indian basin active convective phase (not shown, but results are linear and so opposite those for phases 5-8). Although upper Indian basin MJO convective events (e.g., Ray and Li 2013), upward motion associated with these waves arriving from the west does enhance the development of new MJO convection (Powell and Houze, 2015). The covariance analysis on its own is incapable of distinguishing a reduction of amplitude of positive or negative covariance between reduced amplitude in activity consistent with the same sign, or a stronger mix of activity of the opposite sign, but a full swap in the sign of covariance implies conditions favoring the opposite form.

The findings of reduced total global extent in Kelvin-like signals, and significantly stronger Rossby wave-like height anomalies appear to contradict the conclusions of Abhik et al. (2019), who showed that equatorial wave spectral power does not vary significantly with the QBO outside of the MJO portion of the spectrum. However, these Kelvin and Rossby wave signals are outside of the spectral bands considered thereby, because these signals are timed with the MJO, the dominant signal in the RMM index, while the Kelvin wave signals discussed by Abhik et al. (2019) are inside the Kelvin wave band of Wheeler and Kiladis (1999). Instead, the results presented here represent planetary scale, wavenumber 1-2 Kelvin and Rossby wave signals associated with the MJO. Figure 3 of Abhik et al. (2019) agrees with the present assessment, with substantial increases in spectral power in the MJO band at wavenumbers 1-2 proximate to the Kelvin wave dispersion curve (Also, the plotted dispersion curves in their Figure 3 do not account for Kelvin wave phase speed change in response to advection by the background wind). The Rossby wave-like features within the tropics considered here, such as the cross equatorial cyclone pair over the Atlantic region during phase 7 (Fig. b) during the westerly QBO appear to include stationary and eastward-moving components, so it also occurs outside of the equatorial Rossby wave band considered by Abhik et al. (2019). Comparable vertical cross sections of the MJO-associated circulation structure are

available from Hendon and Abhik (2018). The patterns highlighted here at 200 hPa are consistent with enhanced downward-phase propagation of Kelvin waves during the easterly QBO that are less apparent during the westerly QBO, as in Figures 1-2 of Hendon and Abhik (2018).

These results raise several questions that this paper does not address that require further study. The QBO alters the meridional and vertical shears of the zonal wind between the equatorial stratosphere and the neighboring regions of the subtropical stratosphere and the tropical troposphere. These changes would refract Rossby waves and Kelvin waves crossing the regions differently between the different QBO states. Kelvin wave phase planes propagate downward from the stratosphere as they are forced from energy sources below, so it is plausible that changes in vertical shear of the zonal wind would impact how these phase planes refract into the upper troposphere. Further work is needed to assess whether these changes reduce Kelvin wave variance associated with the MJO during the westerly QBO.

5. Acknowledgements

Funding was provided by the National Science Foundation grant AGS1560627, AGS1757342, and AGS2103624 to Paul Roundy. The daily OLR and reanalysis data were obtained from the NOAA PSD, from the following websites:

https://www.esrl.noaa.gov/psd/data/gridded/data.interp OLR.html and

https://www.esrl.noaa.gov/psd/data/gridded/data.ncep.reanalysis.html. Three reviewers provided feedback that greatly improved the manuscript.

6. References

- Densmore C R, Sanabia E R, Barrett B S. 2019. QBO Influence on MJO Amplitude over the Maritime Continent: Physical Mechanisms and Seasonality, *Mon. Wea. Rev.*, *147*(1), 389-406.
- Elsner JB, Tsonis, AA. 1993. Nonlinear dynamics established in the ENSO. Geophys. Res. Lett., 20: 213-216. https://doi.org/10.1029/93GL00046
- Feng, P., and H. Lin. 2019. Modulation of the MJO-Related Teleconnections by the QBO. Journal of Geophysical Research, D: Atmospheres 124 (22): 12022–33.
- Gahtan, J, Roundy, PE. 2020a. Wavelet isolation of meridionally moving geopotential height perturbations near the subtropics of eastern Africa and their relationship with the Madden–Julian Oscillation. *Q J R Meteorol Soc.* 146: 380–400. https://doi.org/10.1002/qj.3681
- Gahtan, J, Roundy, PE. 2020b. Meridional movement of geopotential height anomalies in the subtropics and the relationship to the base-state flow. *QJR Meteorol*Soc. 1–20. https://doi.org/10.1002/qj.3937
- Haertel, P. 2021: Kelvin/Rossby Wave Partition of Madden-Julian Oscillation Circulations. *Climate*, *9*, 2. https://doi.org/10.3390/cli9010002
- Haynes, P.H. (1998), The latitudinal structure of the quasi-biennial oscillation. Q.J.R. Meteorol. Soc., 124: 2645-2670. https://doi.org/10.1002/qj.49712455206
- Hendon H H, Abhik S. 2018. Differences in vertical structure of the Madden-Julian Oscillation associated with the quasi-biennial oscillation. *Geophysical Research*Letters, 45, 4419–4428. https://doi.org/10.1029/2018GL077207
- Hood LL, Redman M A, Johnson W L, Galarneau Jr, T J. 2020. Stratospheric Influences on the

- MJO-Induced Rossby Wave Train: Effects on Intraseasonal Climate. Journal of Climate, 33(1), 365-389.
- Kiladis GN, Wheeler MC, Haertel PT, Straub KH, Roundy PE. 2009. Convectively coupled equatorial waves, *Rev. Geophys.* 47, RG2003, doi: 10.1029/2008RG000266.
- Klotzbach P, Abhik S, Hendon HH. 2019. On the emerging relationship between the stratospheric Quasi-Biennial oscillation and the Madden-Julian oscillation. *Sci Rep* 9, 2981. https://doi.org/10.1038/s41598-019-40034-6
- Liebmann B, Smith CA, 1996. Description of a complete (interpolated) outgoing longwave radiation datasets. *Bull. Amer. Meteor. Soc.* 77, 1275–1277.
- Madden RA, Julian PR. 1972. Description of Global-Scale Circulation Cells in the Tropics with a 40–50 Day Period, *Journal of Atmospheric Sciences* 29(6), 1109-1123.
- Martin Z, Wang S, Nie J, Sobel A. 2019. The Impact of the QBO on MJO Convection in Cloud-Resolving Simulations, *Journal of the Atmospheric Sciences* 76(3), 669-688.
- Martin, Z., Son, SW., Butler, A. Hendon, H., Kim H, Sobel A, Yoden S., Zhang C., 2021. The influence of the quasi-biennial oscillation on the Madden–Julian oscillation. Nat Rev Earth Environ 2, 477–489.
- Mayer K J, Barnes E A. 2020. Subseasonal Midlatitude Prediction Skill Following Quasi-Biennial Oscillation and Madden–Julian Oscillation Activity. Weather Clim. Dynam., 1, 247–259. https://doi.org/10.5194/wcd-1-247-2020.
- Moore R W, Martius O, Spengler T. 2010. The Modulation of the Subtropical and Extratropical Atmosphere in the Pacific Basin in Response to the Madden–Julian Oscillation, Monthly Weather Review, 138(7), 2761-2779.
- Plumb RA, Bell RC. 1982. A model of the quasi-biennial oscillation on an equatorial beta-plane.

- Q.J.R. Meteorol. Soc. 108, 335-352. https://doi.org/10.1002/qj.49710845604
- Powell SW, Houze RA. 2015. Effect of dry large-scale vertical motions on initial MJO convective onset. *J. Geophys. Res. Atmos.* 120, 4783–4805. doi: 10.1002/2014JD022961.
- Ray P, Li T. 2013. Relative Roles of Circumnavigating Waves and Extratropics on the MJO and Its Relationship with the Mean State, *Journal of the Atmospheric Sciences* 70(3), 876-893.
- Richter J H, Rasch P J 2008. Effects of Convective Momentum Transport on the Atmospheric Circulation in the Community Atmosphere Model, Version 3, *Journal of Climate*, *21*(7), 1487-1499. Retrieved Mar 30, 2021, from https://journals.ametsoc.org/view/journals/clim/21/7/2007jcli1789.1.x
- Roundy, P. E., Schreck, C. J., III, & Janiga, M. A. (2009). Contributions of Convectively

 Coupled Equatorial Rossby Waves and Kelvin Waves to the Real-Time Multivariate MJO

 Indices, *Monthly Weather Review 137*(1), 469-478.
- Roundy PE. 2014. Some Aspects of Western Hemisphere Circulation and the Madden–Julian Oscillation, *Journal of the Atmospheric Sciences* 71(6), 2027-2039.
- Roundy PE. 2017. Diagnosis of seasonally varying regression slope coefficients and application to the MJO. Q.J.R. Meteorol. Soc., 143: 1946-1952. https://doi.org/10.1002/qj.3054
- Roundy PE. 2020. Interpretation of the spectrum of eastward-moving tropical convective anomalies. *Q J R Meteorol Soc.* 146, 795–806. https://doi.org/10.1002/qj.3709
- Sakaeda N, Roundy PE. 2015. The development of upper-tropospheric geopotential height anomaly in the Western Hemisphere during MJO convective initiations. Q.J.R. Meteorol. Soc., 142: 942-956. https://doi.org/10.1002/qj.2696
- Sakaeda, N., Dias, J., & Kiladis, G. N. 2020. The unique characteristics and potential mechanisms of the MJO-QBO relationship. Journal of Geophysical Research: Atmospheres,

- 125, e2020JD033196. https://doi.org/10.1029/2020JD033196
- Straub K H, Kiladis G N. 2003: The Observed Structure of Convectively Coupled Kelvin Waves: Comparison with Simple Models of Coupled Wave Instability, *Journal of the Atmospheric Sciences*, 60(14), 1655-1668.
- Toms B A, Barnes EA, Maloney E D. 2020. The Global Teleconnection Signature of the Madden-Julian Oscillation and Its Modulation by the Quasi-Biennial Oscillation.

 JGRA. https://agupubs.onlinelibrary.wiley.com/doi/abs/10.1029/2020JD032653.
- Wheeler M, Kiladis GN. 1999. Convectively Coupled Equatorial Waves: Analysis of Clouds and Temperature in the Wavenumber–Frequency Domain. *J. Atmos. Sci.* 56, 374–399, doi:10.1175/1520-0469(1999)056<0374:CCEWAO>2.0.CO;2.
- Yoo C, Son SW. 2016. Modulation of the boreal wintertime Madden-Julian oscillation by the stratospheric quasi-biennial oscillation, *Geophys. Res. Lett.* 43, 1392–1398, doi:10.1002/2016GL067762.
- Wang, B, Xie, X, 1997: A Model for the Boreal Summer Intraseasonal Oscillation, *Journal of the Atmospheric Sciences*, 54(1), 72-86.
- Weare, BC, 2010: Madden-Julian Oscillation in the tropical stratosphere, *J. Geophys. Res.*, 115, D17113, doi:10.1029/2009JD013748.
- Wheeler MC, Hendon HH. 2004. An All-Season Real-Time Multivariate MJO Index:

 Development of an Index for Monitoring and Prediction, *Monthly Weather Review 132*(8), 1917-1932.
- Zhang C. 2005. Madden-Julian Oscillation, *Rev. Geophys.* 43, RG2003, doi:10.1029/2004RG000158.
- Zhang C, Zhang B. 2018. QBO-MJO connection. *Journal of Geophysical Research*:

Atmospheres 123, 2957–2967. https://doi.org/10.1002/2017JD028171

Table 1				
RMM Phase	1 & 5	2 & 6	3 & 7	4 & 8
QBOe	5.6	6.0	8.1	9.2
QBOw	36.2	12.9	31	33.7

Table 1 Global average regressed height variance by RMM Phase and QBO easterly or westerly, including only significantly different regions. Units: m².

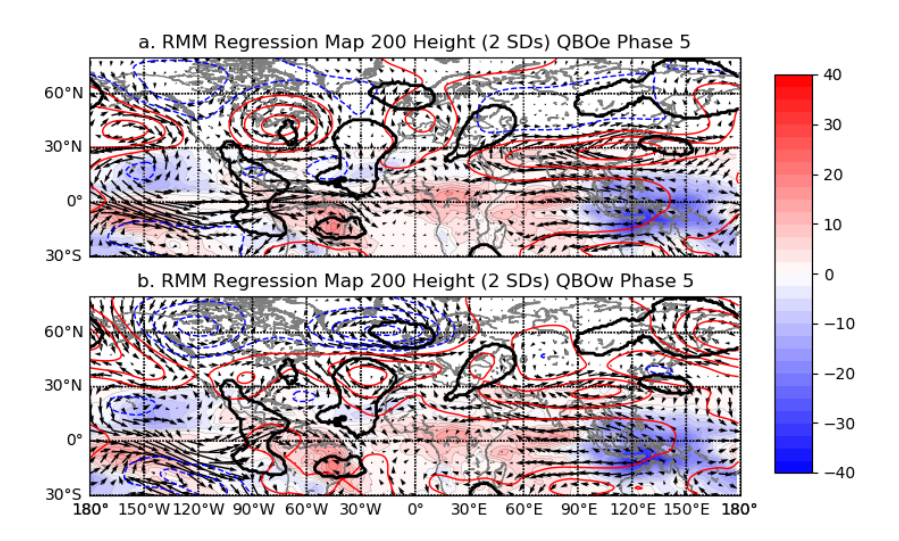


Figure 1: 200 hPa geopotential height (contours, 10m interval, solid, positive, dashed and negative contours are available in red and blue online) and wind anomalies (vectors), together with OLR anomalies, (shading, Wm⁻², with fine solid black contours indicating positive anomalies with fine dashed contours indicating negative anomalies) regressed against the RMM index and reconstructed for the indicated RMM phases, given the QBO index at -10 m s⁻¹. Black contours enclose regions of height anomalies that are significantly different between panels a and b at the 95% level.

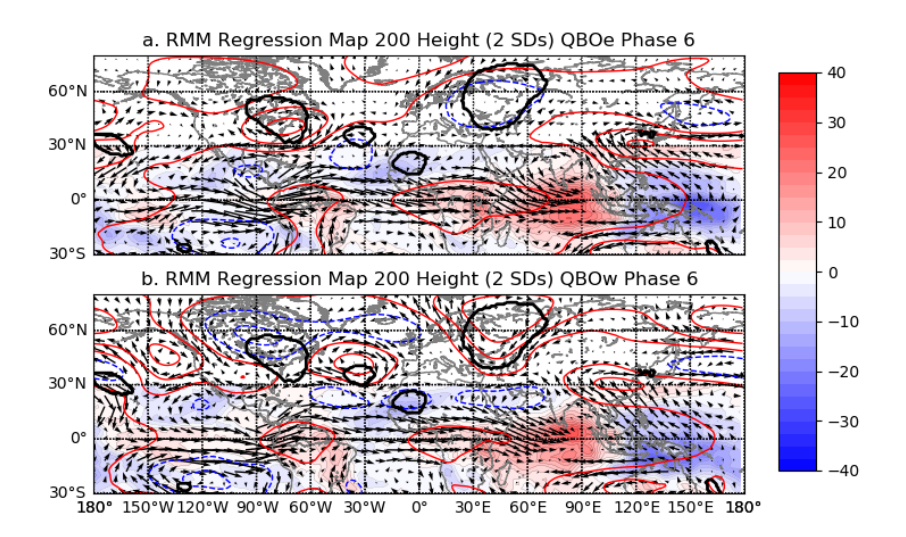


Figure 2: Same as Figure 1, except for RMM phase 6.

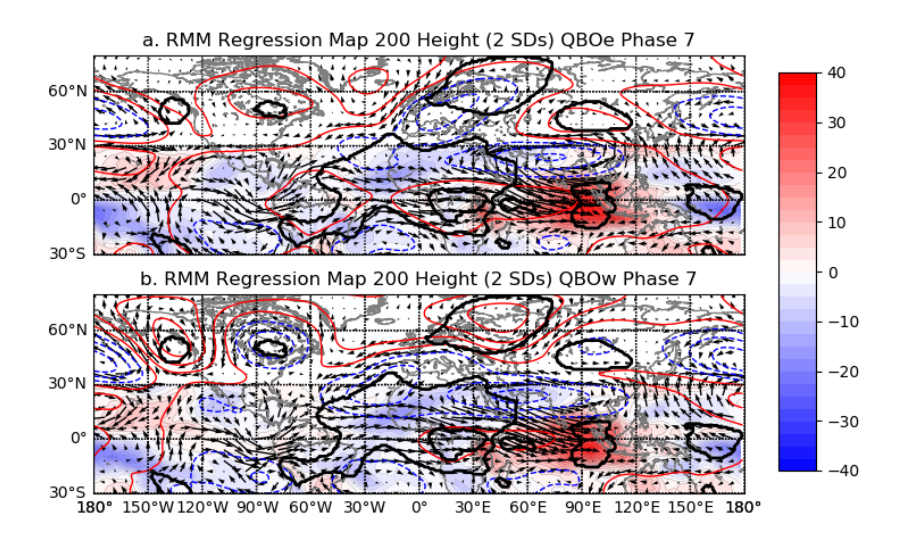


Figure 3, Same as Fig. 1, except for RMM phase 7.

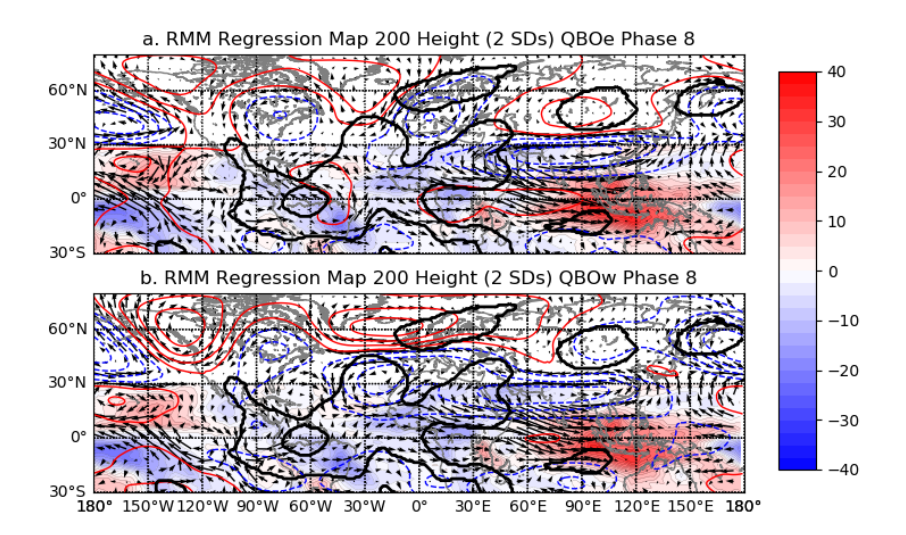


Figure 4, Same as Fig. 1, except RMM phase 8.

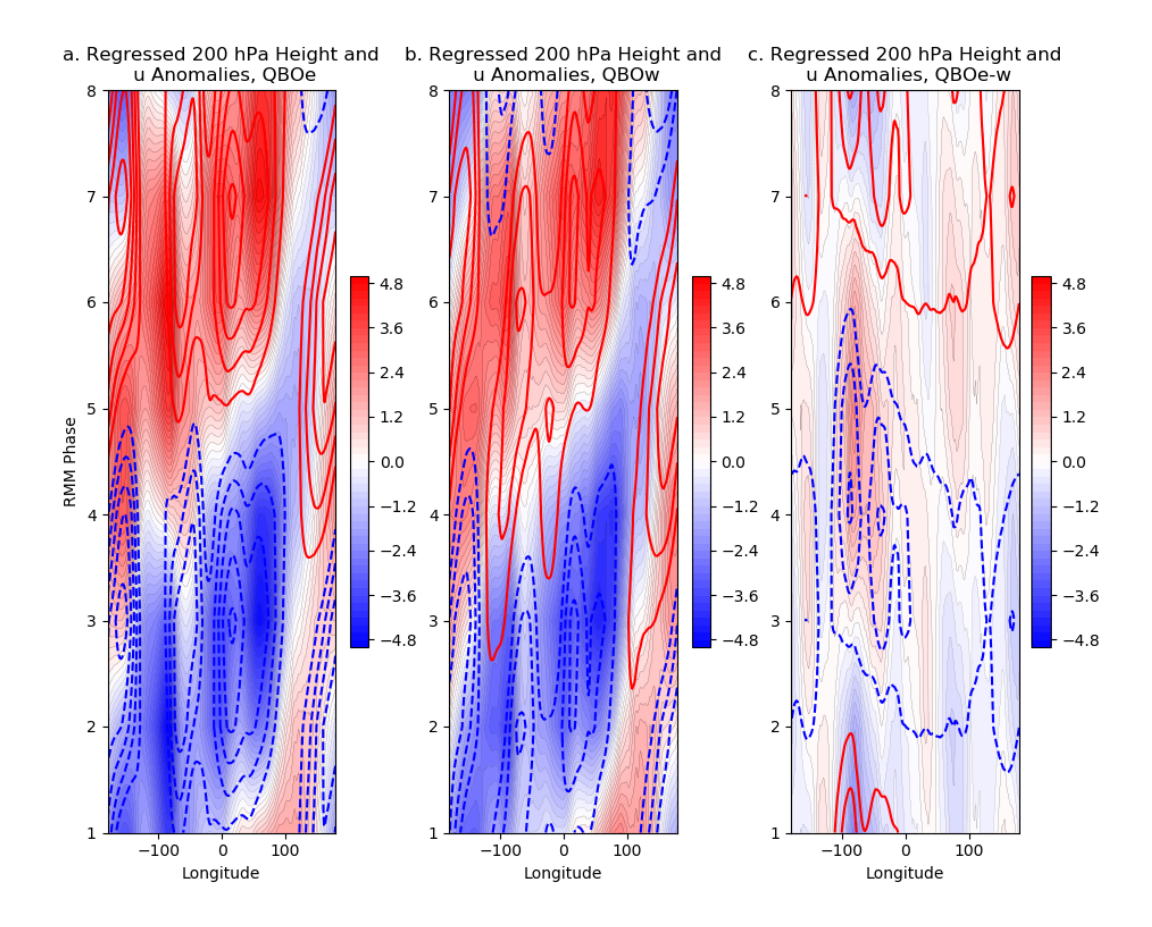


Figure 5: Zonal wind anomaly (shading, m s⁻¹, with color available online, and fine contours included, with solid indicating positive and dashed negative), and geopotential height anomaly (heavy contours, 2m interval, with the zero contour omitted, with dashed negative and solid positive), averaged from 10°S to 10°N for (a) easterly QBO (–10m s⁻¹), (b) westerly QBO (+10m s⁻¹), and (c) easterly minus westerly QBO. Results are from the same regressions plotted in Figures 1-4.

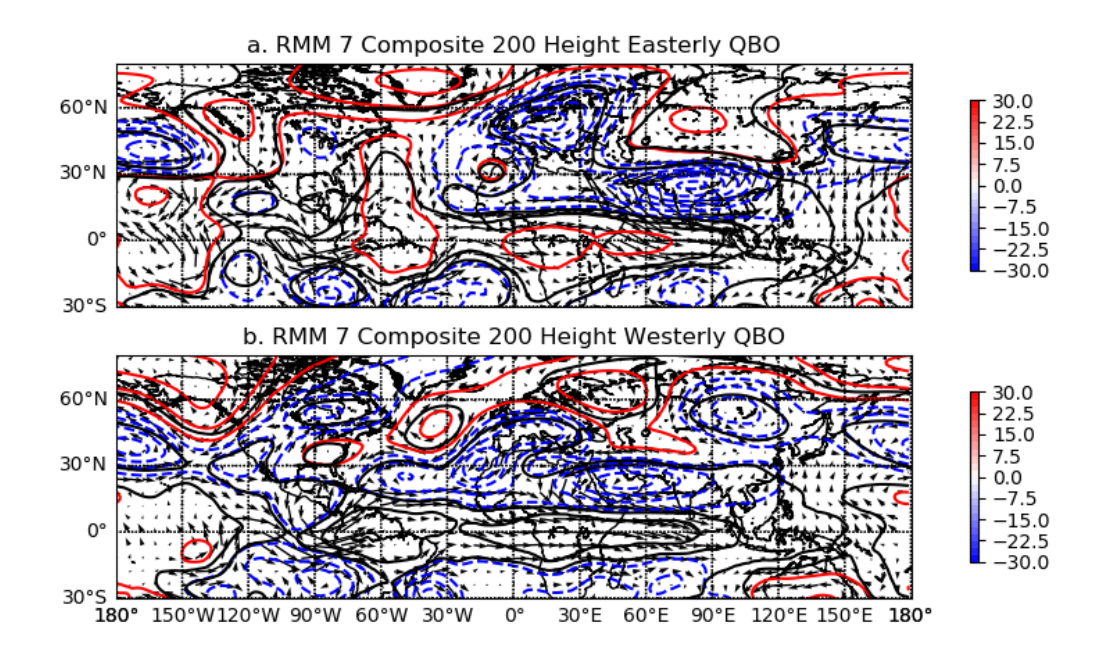


Figure 6: Composite average 200 hPa height anomalies (contours, interval=5 m s⁻¹, with dashed representing negative anomalies) and wind anomalies (vectors) for all days corresponding to December through February RMM 7 > amplitude 0.5 during (a), QBO index < -4 m s⁻¹ and (b), QBO index > +4m s⁻¹. Black contours enclose regions of composite height anomalies that are significantly different from zero at the 95% level.

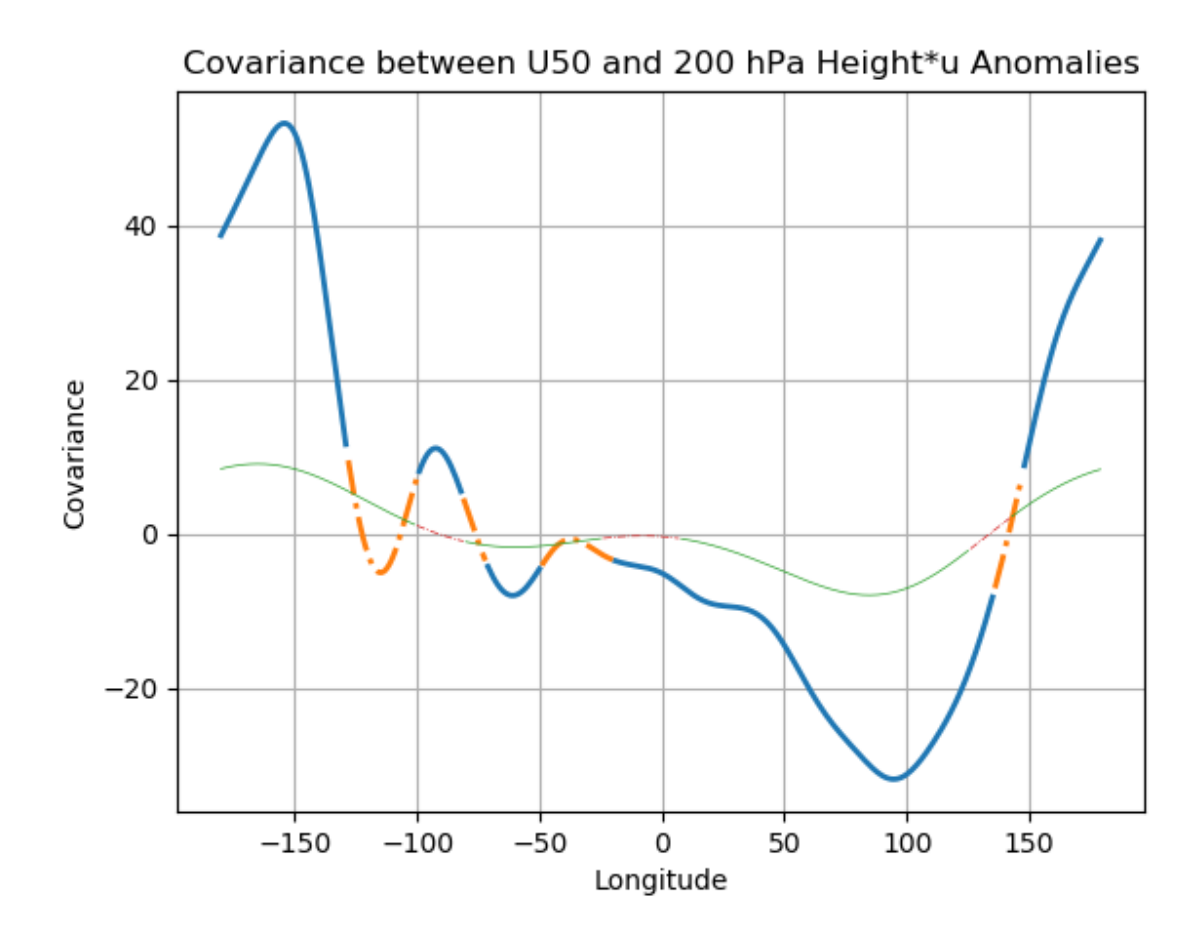


Figure 7: Covariance between the smoothed zonal mean 50 hPa zonal wind index and time series at each grid point that represent the product of MJO-filtered 200 hPa geopotential height and zonal wind anomalies. Units are m m s⁻¹ m s⁻¹. Includes data from December through February. Heavy curve includes wavenumbers 1-9. Thin curve includes wavenumbers 1-2. Dash-dotted portions are not statistically different from zero following the student's t-test.